JOURNAL OF VIROLOGY, July 2007, p. 7099–7110 Vol. 81, No. 13
0022-538X/07/$08.00+0 doi:10.1128/JVI.00272-07

Human Immunodeficiency Virus Type 1 cDNAs Produced in the Presence of APOBEC3G Exhibit Defects in Plus-Strand DNA Transfer and Integration▽†

Jean L. Mbisa,[1] Rebekah Barr,[1] James A. Thomas,[2] Nick Vandegraaff,[3] Irene J. Dorweiler,[4] Evguenia S. Svarovskaia,[1]‡ William L. Brown,[4,5] Louis M. Mansky,[4] Robert J. Gorelick,[2] Reuben S. Harris,[4,5] Alan Engelman,[3] and Vinay K. Pathak[1]*

HIV Drug Resistance Program[1] and AIDS Vaccine Program,[2] SAIC-Frederick, Inc., National Cancer Institute-Frederick, Frederick, Maryland 21702-1201; Department of Cancer Immunology and AIDS, Dana-Farber Cancer Institute and the Division of AIDS, Harvard Medical School, Boston, Massachusetts 02115[3]; University of Minnesota, Departments of Diagnostic and Biological Sciences and Microbiology and Institute for Molecular Virology, Minneapolis, Minnesota 55455[4]; and University of Minnesota, Department of Biochemistry, Molecular Biology and Biophysics, Arnold and Mabel Beckman Center for Transposon Research, Minneapolis, Minnesota 55455[5]

Received 8 February 2007/Accepted 5 April 2007

Encapsidation of host restriction factor APOBEC3G (A3G) into *vif*-deficient human immunodeficiency virus type 1 (HIV-1) blocks virus replication at least partly by C-to-U deamination of viral minus-strand DNA, resulting in G-to-A hypermutation. A3G may also inhibit HIV-1 replication by reducing viral DNA synthesis and inducing viral DNA degradation. To gain further insight into the mechanisms of viral inhibition, we examined the metabolism of A3G-exposed viral DNA. We observed that an overall 35-fold decrease in viral infectivity was accompanied by a five- to sevenfold reduction in viral DNA synthesis. Wild-type A3G induced an additional fivefold decrease in the amount of viral DNA that was integrated into the host cell genome and similarly reduced the efficiency with which HIV-1 preintegration complexes (PICs) integrated into a target DNA in vitro. The A3G C-terminal catalytic domain was required for both of these antiviral activities. Southern blotting analysis of PICs showed that A3G reduced the efficiency and specificity of primer tRNA processing and removal, resulting in viral DNA ends that are inefficient substrates for integration and plus-strand DNA transfer. However, the decrease in plus-strand DNA transfer did not account for all of the observed decrease in viral DNA synthesis associated with A3G. These novel observations suggest that HIV-1 cDNA produced in the presence of A3G exhibits defects in primer tRNA processing, plus-strand DNA transfer, and integration.

Multiple guanosine (G)-to-adenosine (A) substitutions occurring in retroviral genomes were first observed in spleen necrosis virus, a phenomenon that was named hypermutation by the authors (34); later, similar G-to-A hypermutations were observed in human immunodeficiency virus type 1 (HIV-1) genomes (10, 45). The mechanism of hypermutation remained unclear until the recent discovery that encapsidation of the host cytidine deaminase apolipoprotein B mRNA-editing enzyme-catalytic polypeptide-like 3G (APOBEC3G [A3G]) into HIV-1 virions results in a postentry block to virus replication (39). This block has been attributed mainly to the ability of A3G to deaminate cytidines to uridines in the nascent minus-strand DNA, resulting in G-to-A hypermutations in the provirus (13, 14, 23, 26, 54). The presence of A3G has resulted in G-to-A hypermutation of HIV-1 genomes in cell-based assays that is similar to the hypermutations observed in patient-derived HIV-1 genomes, providing additional evidence that hypermutation contributes to inhibition of retroviruses by A3G (1, 10, 23). The HIV-1 viral infectivity factor (Vif) protein suppresses virion incorporation of A3G by forming a Vif-A3G-E3 ligase complex, which triggers the polyubiquitination and degradation of A3G by the 26S proteasome (8, 22, 29, 53).

A3G contains two zinc-binding motifs, also referred to as catalytic domains (CDs), with the consensus amino acid sequence -His-(Ala/Pro)-Glu-X_{28}-Pro-Cys-X_2-Cys- (HECC) (16, 17). Single amino acid substitutions of the HECC motif in the N-terminal (CD1) or C-terminal (CD2) catalytic domain and the use of APOBEC3F/A3G chimeric proteins have shown that cytidine deaminase activity is primarily associated with CD2 (12, 30, 31). In contrast, CD1 has been implicated in RNA binding and viral encapsidation (30). CD2 also confers the sequence specificity for A3G cytidine deamination, which is a CC dinucleotide on the minus-strand DNA (or a GG on the plus-strand DNA); deamination most frequently results in replacement of the first G with A (12, 13, 26, 31, 54).

Although direct inactivation of viral genomes by G-to-A hypermutation is considered the de facto antiretroviral mechanism of A3G, several other mechanisms are proposed to play a role. First, some reports of A3G CD2 mutants (i.e., catalytic site mutants) have indicated that these variants still retain partial or complete antiviral activity (31, 40). These studies have suggested that A3G possesses an antiretroviral function that is independent from its cytidine deamination activity. Second, A3G may inhibit HIV-1 DNA replication by either promoting DNA degradation or inhibiting DNA synthesis (2, 15,

* Corresponding author. Mailing address: HIV Drug Resistance Program, National Cancer Institute-Frederick, P.O. Box B, Bldg. 535, Rm. 334, Frederick, MD 21702-1201. Phone: (301) 846-1710. Fax: (301) 846-6013. E-mail: vpathak@ncifcrf.gov.

† Supplemental material for this article may be found at http://jvi.asm.org.

‡ Present address: Gilead Sciences, Inc., Durham, NC 27707-3458.

▽ Published ahead of print on 11 April 2007.

26, 28, 41, 46). It has been proposed that removal of the uracil base by uracil DNA glycosylase followed by endonucleolytic cleavage of the abasic site by apurinic-apyrimidinic (AP) endonucleases could decrease viral DNA replication and contribute to the antiretroviral mechanism of A3G (13). In support of this hypothesis, the host uracil DNA glycosylase-2 (UNG2) is incorporated into HIV-1 virions via its interaction with HIV-1 viral protein R (Vpr) (27) and/or integrase (IN) (49). Additionally, degradation of viral DNAs before integration in the presence of A3G has been reported (26, 28). UNG2 has also been reported to facilitate replication of HIV-1 in macrophages (7, 37); however, other recent studies have reported that Vpr prevents virion incorporation of UNG2 by inducing its degradation (38) and that UNG2 does not play a significant role in the antiretroviral activity of A3G (19). Lastly, A3G has been reported to decrease viral DNA accumulation (26), and uracil-containing DNA substrates have shown a defect in plus-strand DNA synthesis initiation (21); both of these defects could result in a decrease in HIV-1 DNA replication. The relative importance of all of these mechanisms to the inhibition of retroviral replication by A3G has not yet been fully elucidated.

In order to gain more insights into the mechanisms by which A3G blocks retroviral replication, we set out to analyze the metabolism of viral DNA from its synthesis to integration using a variety of quantitative real-time PCR-based assays. Our results show that A3G inhibits both viral DNA accumulation and integration. The inhibition of both viral DNA accumulation and integration was dependent on a functional CD2 and did not involve degradation of viral DNA by UNG2. Our studies also show that the presence of A3G results in the formation of aberrant viral 3′ long terminal repeat (LTR) DNA ends, suggesting that A3G interferes with cleavage and removal of the primer tRNA. We hypothesize that the aberrant viral DNA ends result in a defect in integration and contribute to the defect in DNA synthesis by inhibiting plus-strand DNA transfer.

MATERIALS AND METHODS

Plasmids. The HIV-1-based vector pHDV-eGFP as well as the HIV-1 helper constructs pC-Help and pC-HelpΔ*vif*, pHCMV-G, pcDNA-APO3G, pA3G-D128Kcmyc, and pD64E have been previously described (20, 43, 51). pHDV-eGFP expresses HIV-1 Gag-Pol proteins and enhanced green fluorescent protein (eGFP). The HIV-1 helper construct pC-HelpΔ*vif*Δ*vpr* is identical to pC-HelpΔ*vif*, except that the Vpr open reading frame was eliminated by mutation of the AUG initiation codon. pDNA3.1-A3G(E259>Q) and pA3G-C288Scmyc were constructed using the QuikChange site-directed mutagenesis kit (Stratagene) and confirmed by DNA sequencing.

Cells, transfections, and virus production. The human 293T cell line was obtained from the American Type Culture Collection (ATCC) and maintained as previously described (32). The 293T 91-26 cell line is an internal ribosome entry site-Zeo-expressing clone of 293T cells. The 293T 91-26 4D2 cell line is a derivative of the 293T 91-26 cell line that expresses a UNG2 inhibitor protein (Ugi). Virus stocks were prepared by transfection of 293T 91-26 or 293T 91-26 4D2 cells, seeded at a density of 5×10^6 cells per 100-mm-diameter dish, with pHDV-eGFP, pHCMV-G, one of the three helper vectors (pC-Help, pC-HelpΔ*vif*, or pC-HelpΔ*vif*Δ*vpr*), or pc-DNA-APO3G (or salmon sperm DNA) using a CalPhos Mammalian Transfection kit (BD Biosciences). For real-time PCR experiments, the transfected cell monolayers were rinsed with phosphate-buffered saline containing 1% fetal calf serum three times each at 6 and 24 h posttransfection and once at 30 h posttransfection to reduce or eliminate contamination with transfected pHDV-eGFP DNA. Virus supernatants were harvested at 48 h posttransfection, clarified by centrifugation, filtered through 0.45-μm filters, and quantified by p24 enzyme-linked immunosorbent assay (Perkin-Elmer).

Infections and viral DNA quantification by real-time PCR. 293T cells were seeded at a density of 10^5 cells per 60-mm-diameter dish and 24 h later were infected with equal amounts of HIV-1 p24 capsid-normalized virus samples for 3 h as previously described (32). A duplicate of each virus sample was heat inactivated at 65°C for 1 h and used to infect cells in parallel as a background control to determine the level of contamination with transfected DNA. Cells were harvested at 6, 24, and 120 h after infection, and total cellular DNA was extracted using a QIAamp DNA Blood Mini kit (QIAGEN). The DNA was then digested with DpnI (NEB), which digests methylated plasmid DNA but does not digest viral or cellular DNA, to further reduce plasmid DNA contamination. The amounts of unintegrated viral DNA, proviruses, and 2-LTR circles were quantified using the ABI Prism 7700 sequence detection system as previously described (3, 44, 47). Briefly, the copy numbers in each sample were adjusted for DNA input by quantification of cellular porphobilinogen dehydrogenase gene (PBGD) copy numbers and subtraction of background signal determined by infection with heat-inactivated virus. The primer-probe sets were purchased from Integrated DNA Technologies and are listed in Table S1 in the supplemental material. Cells were also harvested at 48 h after infection and analyzed by flow cytometry (FACScan; Becton Dickinson) for expression of eGFP to determine the efficiency of infection.

UDG activity assays. We performed uracil DNA glycosylase (UDG) activity assays, which are designed to determine the enzymatic activity of all uracil DNA glycosylases in cells, including UNG2. 293T, 293T 91-26, or 293T 91-26 4D2 whole-cell lysates were prepared using HED buffer (25 mM HEPES, 5 mM EDTA, 1 mM dithiothreitol, 10% glycerol, pH 7.8, containing Complete Protease Inhibitor [Roche]) and analyzed for UDG activity as described previously (9). Briefly, whole-cell extracts were incubated with 1 pmol of fluorescein isothiocyanate (FITC)-labeled deoxyoligonucleotide substrate (UDG-F) containing a single uracil base at position 16 (see Table S1 in the supplemental material) in a final volume of 10 μl at 37°C for 2 h and analyzed by denaturing gel electrophoresis. The existing AP endonuclease activity present in the extracts was sufficient to cleave all of the deglycosylated substrate generated during the reaction. Recombinant uracil-DNA glycosylase (0.1 U; Roche) and Ugi (2 U; NEB) were used as controls.

To monitor UDG activity in virus particles, oligonucleotide TU13 (see Table S1 in the supplemental material) containing a single uracil base at position 13 was 5′-end labeled with [γ-^{32}P]ATP using a DNA 5′-end labeling kit and following the manufacturer's directions (Promega). The reaction mixture was then added to a Sephadex G-50 column (Roche) and centrifuged at 1,100 × *g* for 4 min. A 3-μl volume of cell culture supernatant from virus-producing cells was mixed with 1.5 μl of 10× UDG buffer (200 mM Tris-HCl, 10 mM EDTA, 10 mM dithiothreitol, pH 8.0), 1 μl of radioactively labeled TU13, and H_2O to a final volume of 15 μl. The reaction mixture was incubated at 37°C for 2 h, the phosphodiester backbone was hydrolyzed by the addition of 5 μl of 0.5 M NaOH and boiling for 30 min, and the mixture was analyzed by denaturing gel electrophoresis.

Western blotting analysis. Virions were concentrated by ultracentrifugation, adjusted to equivalent amounts using an HIV-1 p24 enzyme-linked immunosorbent assay kit (Perkin Elmer), and used for Western blotting analysis as previously described (51). A3G proteins were detected using ApoC17 rabbit polyclonal antibody (a kind gift from Klaus Strebel) generated against the C-terminal 17 amino acids of A3G.

PIC isolation and real-time quantitative PCR assay for PIC function. To isolate preintegration complexes (PICs), 293T cells were seeded at a density of 3×10^6 cells per 100-mm-diameter dish and 24 h later were infected with virus for 7 h. Cells were harvested by washing twice in buffer $K^{-/-}$ (20 mM HEPES, pH 7.6, 150 mM KCl, 5 mM $MgCl_2$) and lysed in buffer $K^{+/+}$ (buffer $K^{-/-}$ plus 0.025% [wt/vol] digitonin, 1 mM dithiothreitol, and 20 μg/ml aprotonin) for 10 min at room temperature. Supernatant was collected by sequential centrifugation at 1,500 × *g* for 4 min and 19,000 × *g* for 1 min at 4°C and treated with RNase A (20 μg/ml). The real-time quantitative PCR assay for PIC function was carried out essentially as previously described (25), with the addition of an RU5-specific TaqMan probe (AE995; see Table S1 in the supplemental material) to increase the sensitivity of detecting second-round PCR products.

Sequencing analysis of 2-LTR circle junctions. 293T cells seeded at a density of 2×10^5 cells per 60-mm-diameter dish were infected 24 h later with either wild-type virus or Δ*vif* HIV-1 produced in the presence of A3G. Total cellular DNA isolated from infected cells at 24 h after infection was PCR amplified to obtain fragments encompassing the 2-LTR circle junction (full-length junctions are 336 bp). The PCR primers are described in Table S1 in the supplemental material (18). The PCR products were purified by a PCR purification kit

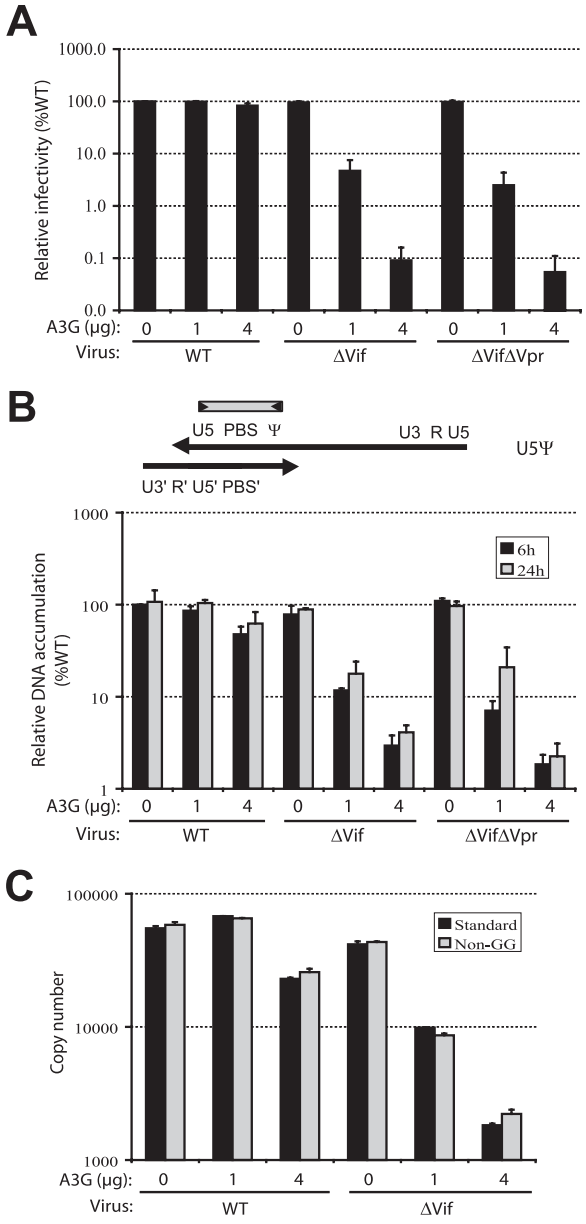

FIG. 1. Effect of A3G on viral infectivity and DNA synthesis. (A) Flow cytometry analysis of the effects of different amounts of A3G on pHDV-eGFP wild-type (WT), Δ*vif*, and Δ*vif*Δ*vpr* viral infection. The viruses were produced in the absence or presence of 1 or 4 μg of pcDNA-APO3G during cotransfection of 293T cells with the viral expression constructs. The MOI was determined from the proportion of GFP^+ cells after infection; WT virus in the absence of A3G yielded 43 to 86% GFP^+ cells (MOI set to 100%). (B) Late RT product levels determined at 6 h (black bars) or 24 h (gray bars) postinfection with WT, Δ*vif*, or Δ*vif*Δ*vpr* virus in the absence or presence of 1 or 4 μg of pcDNA-APO3G. WT viral DNA accumulation at 6 h postinfection in the absence of A3G was set to 100%; these copy numbers were 31,608 and 21,607 in two independent experiments after adjustment for input DNA, determined by quantifying host PBGD gene copies and subtraction of background signal from a parallel infection with heat-inactivated virus, which was <200 copies. The schematic shows the relative locations of U5 and Ψ primers and probe (shaded gray box containing arrows) above the plus and minus DNA strands (top and bottom long arrows, respectively). (C) Comparison of amounts of late RT products quantified by either the Standard U5Ψ primer-probe set (black bars), which contains GG dinucleotides, or the Non-GG U5Ψ primer-probe set (gray bars). Viral DNA levels were determined at 24 h after infection with WT or Δ*vif* virus produced in the absence or presence of 1 or 4 μg of pcDNA-APO3G. Error bars in all graphs represent the standard errors of the means of two independent experiments.

(QIAGEN) and cloned into pCR2.1-TOPO vector (Invitrogen). Plasmid DNA was isolated from individual bacterial colonies using a BioRobot 9600 (QIAGEN) and sequenced using the M13 sequencing primer (Macrogen Inc.).

Southern blotting analysis of HIV-1 viral DNA ends in PICs. 293T cells were seeded at a density of 5×10^6 cells per 100-mm-diameter dish and infected 24 h later with Δ*vif* HIV-1 produced in the presence or absence of A3G. Cytoplasmic DNA was extracted 6 h after infection as described for PIC isolation. The DNA samples were digested with HindIII, resolved by electrophoresis through a denaturing polyacrylamide gel, transferred to a Duralon-UV membrane (Stratagene), and analyzed by Southern blotting as described previously (43).

Statistical analysis. We used the paired two-tailed Student *t* test to determine if infectivity, DNA accumulation levels, integration efficiency, or 2-LTR circles were significantly different between two viruses. The null hypothesis was rejected in favor of the alternative hypothesis if the *P* value was above the chosen significance threshold level of 0.05.

RESULTS

A3G inhibits Δ*vif* viral DNA synthesis in a dose-dependent manner. It has been reported that A3G reduces viral DNA levels by inducing degradation and inhibiting viral DNA synthesis (2, 11, 15, 26, 28, 41, 46). To determine the effects of A3G on HIV-1 DNA replication, wild-type and Δ*vif* viruses were produced in the absence or presence of different amounts of A3G. 293T cells were cotransfected with pHDV-eGFP, pC-Help, or pC-Help-Δ*vif* (Gag and Gag-Pol expression plasmids that either express or do not express Vif, respectively), pH-CMV-G (a plasmid that expresses vesicular stomatitis virus protein G), and pcDNA-APO3G (a plasmid that expresses human A3G). Infection of 293T target cells with the transfection-derived viruses resulted in a single round of replication; the infection rate was determined by analyzing the level of GFP expression using flow cytometry. The multiplicity of infection (MOI) of wild-type (Vif^+) virus in the absence of A3G ranged from 0.57 to 1.99. The effect of A3G on Δ*vif* viral replication was compared with that of the wild-type virus in the absence of A3G (set at 100%) (Fig. 1A). Cotransfection of 1 μg of pcDNA-APO3G reduced Δ*vif* virus infectivity to 2.7% (35-fold decrease), while 4 μg of pcDNA-APO3G resulted in a 1,000-fold reduction in infectivity. In contrast, cotransfection with pcDNA-APO3G did not significantly affect the infectivity of wild-type virus. The dose-dependent effect of A3G on infectivity is consistent with previous reports (26, 39, 40).

Next, total cellular DNA was isolated from infected cells at 6 and 24 h after infection, and viral DNA was quantified by real-time PCR using a standard late reverse transcription (RT) product primer-probe set, which detects viral DNA product after the plus-strand DNA transfer step in reverse transcription (Fig. 1B, top schematic; also see Table S1 in the supplemental material). The effect of A3G on the Δ*vif* viral DNA level was compared to of wild-type virus in the absence of A3G (set at 100%, 6-h time point) (Fig. 1B). The viral DNA amount was decreased in Δ*vif* virus by seven- and fivefold in the presence of 1 μg of pcDNA-APO3G at 6 and 24 h after infection, respectively ($P \leq 0.02$; *t* test). The viral DNA amount was decreased more drastically (22- to 26-fold) in the presence of 4 μg of pcDNA-APO3G. In contrast, accumulation of viral DNA

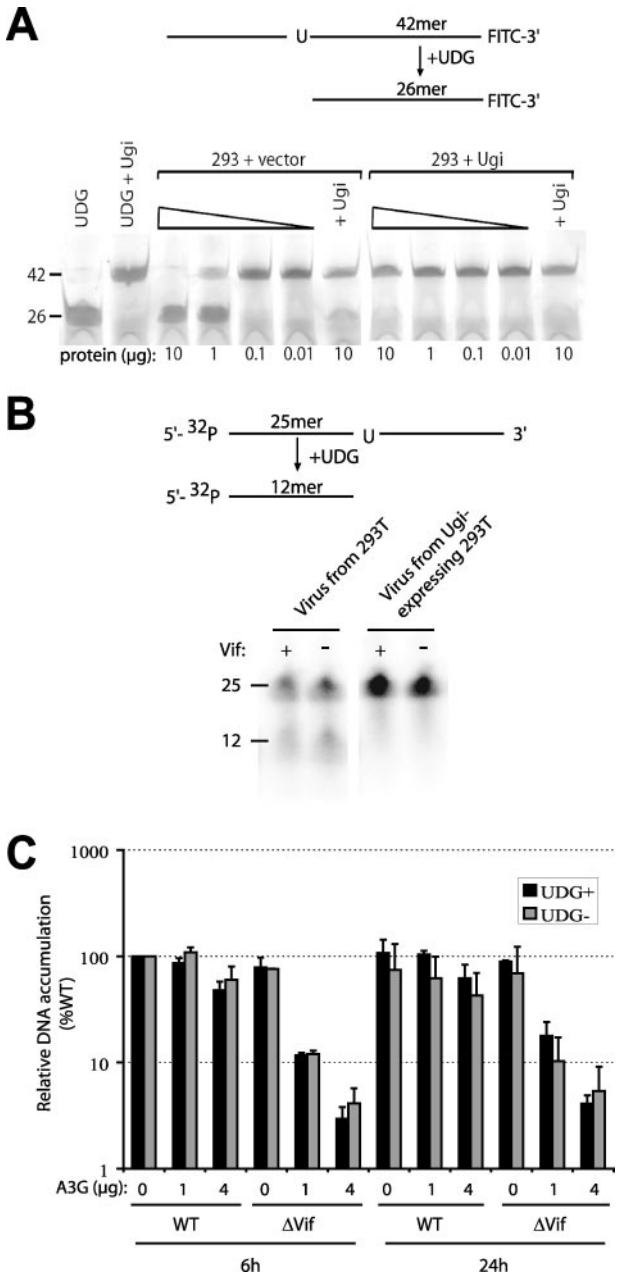

FIG. 2. Effect of inactivating UNG2 in virus producer cells on viral DNA replication. (A) Uracil-DNA excision activity in 293T cells stably transfected with Ugi. A fluorescein-labeled oligonucleotide containing a single dU residue was incubated in the presence of recombinant UDG or serial dilutions of 293T cell lysate (10, 1, 0.1, or 0.01 μg protein). The first two lanes show the effect of recombinant UDG or UDG + Ugi, respectively. (B) Assay of virus-associated uracil DNA glyosylase activity. Cell culture supernatants from virus-producing cells (293T cells or Ugi-expressing 293T cells) were incubated with a 5′-end-labeled 26-mer oligonucleotide composed of thymidine with a uracil base at position 13 in UDG buffer for 2 h at 37°C and subsequent addition of NaOH and boiling to destroy any apurinic sites created by UDG activity. (C) Comparison of relative amounts of late RT products in cells infected with wild-type (WT) or Δ*vif* virus produced in 293T cells (black bars) or Ugi-expressing 293T cells (gray bars) in the absence or presence of 1 or 4 μg of pcDNA-APO3G. Viral DNA levels were determined at 6 or 24 h after infection, and the amount of viral DNA accumulated in cells infected with WT virus in the absence of A3G was set to 100%; these copy numbers ranged from 64,360 to 209,768 in two independent experiments after adjustment for input DNA determined by quantification of host PBGD gene copies and subtraction of the background from a parallel infection with heat-inactivated virus, which was <600 copies. Error bars represent the standard errors of the means of two independent experiments.

was not significantly affected for the Δ*vif* virus in the absence of A3G or wild-type virus in the presence of both 1 and 4 μg of pcDNA-APO3G. These results showed that when A3G expression reduced the rate of viral infection 35-fold, viral DNA accumulation was reduced approximately five- to sevenfold; in addition, the effect of A3G on Δ*vif* viral DNA accumulation was dose dependent.

Sequence analyses of viral DNAs synthesized in the presence of A3G have indicated that approximately 87% of the G-to-A substitutions occur in GG dinucleotides (24). To rule out the possibility that quantification of viral DNA late RT products was affected by decreased hybridization of primer-probe sets to hypermutated DNA, we designed a second primer-probe set that lacked GG dinucleotides in the forward primer or probe or CC dinucleotides in the reverse primer (see Table S1 in the supplemental material). Quantification of viral DNA by this primer-probe set (Non-GG) was compared with that by the original primer-probe set (Standard). The comparison showed that there was no significant difference in the amount of viral DNA quantified by both primer-probe sets in all samples, particularly Δ*vif* virus in the presence of A3G (Fig. 1C). Thus, the observed decrease in DNA amounts using the Standard primer-probe set was not a consequence of hypermutation of the target DNA; nonetheless, all subsequent quantification of viral DNA levels presented in this study was performed using the Non-GG primer-probe set.

A3G decreases Δ*vif* viral DNA accumulation independent of Vpr or UNG2. It has been proposed that the action of UNG2 creates abasic sites that target viral DNA for degradation (13). Two different approaches were employed to explore whether the decrease in Δ*vif* viral DNA replication in the presence of A3G was due to DNA degradation by UNG2. First, Vpr has been shown to either facilitate or suppress virion incorporation of UNG2 (27, 38); we therefore determined whether deletion of Vpr affected viral DNA levels. The infectivity of Δ*vif*Δ*vpr* virus was comparable to that of Δ*vif* virus in the absence or presence of 1 or 4 μg of pcDNA-APO3G (Fig. 1A). Furthermore, Δ*vif*Δ*vpr* and Δ*vif* viruses generated similar levels of late RT DNA products (Fig. 1B). For example, viral DNA accumulation was decreased by 16-fold and 7-fold at 6 h after infection and by 5-fold and 5-fold at 24 h after infection by Δ*vif*Δ*vpr* and Δ*vif* viruses, respectively, in the presence of 1 μg of pcDNA-APO3G ($P \geq 0.50$; *t* test). These results indicated that Vpr did not significantly affect Δ*vif* viral DNA accumulation in the presence of A3G.

Second, we determined whether the direct inactivation of UNG2 in virus producer cells affected viral DNA synthesis in target cells after infection. To this end, a 293T-based cell line, 293T 91-26-4D2, was constructed to overexpress a known cellular UNG2 inhibitor, Ugi (48). This cell line has UDG activity that is less than 1% of that of the parental 293T cell line (Fig. 2A). To verify that UNG2 was incorporated into the Δ*vif* vi-

ruses, we determined the UDG activities in wild-type and Δ*vif* viruses produced either in control 293T cells or in the Ugi-expressing cells (Fig. 2B). The results indicated that UDG activity was readily detectable in both viruses produced in the control 293T cells but not in Ugi-expressing cells. Viral DNA levels in target cells infected with Δ*vif* virus produced in the Ugi-expressing cell line were not significantly different from those in target cells infected with Δ*vif* virus produced in the control 293T cells expressing an empty vector (Fig. 2C). Thus, the presence of UDG activity in virions did not affect late RT product levels in the presence or absence of A3G. In addition, a comparison of the viral DNA levels after infection of UNG^+ and UNG^- cells with virus produced from UNG^- cells revealed no differences in DNA accumulation, indicating that the presence of UNG2 activity in the target cells of infection does not influence steady-state amounts of viral DNA (data not shown).

A3G decreases the levels of viral DNA integration. The expression of 1 μg of pcDNA-APO3G resulted in a 35-fold decrease in the infectivity of Δ*vif* virus (Fig. 1A), of which only five- to sevenfold was accounted for by a decrease in viral DNA synthesis (Fig. 1B). To determine whether additional post-DNA synthesis steps in viral replication were inhibited by A3G, we investigated the efficiency of viral DNA integration in the presence or absence of A3G. Total cellular DNA was isolated from infected cells 5 days after infection, and the amount of integrated viral DNA was quantified using an Alu-LTR real-time PCR assay (4). Although viral DNA integration is normally completed 36 to 48 h after infection (4), the 5-day time point was selected to ensure analysis of an overall rather than kinetic effect of A3G on levels of integrated DNA. To calculate integration efficiency, the integrated viral DNA copies were expressed as a proportion of the late RT DNA products at 6 h after infection (when viral DNA accumulation is at or near maximum). Wild-type viral DNA integration efficiency in the absence of A3G was 12.3% ± 0.15%, which agrees well with previously published results (4). The integration efficiency of the Δ*vif* virus produced in the presence of 1 μg of pcDNA-APO3G was reduced approximately fivefold compared to Δ*vif* virus in the absence of pcDNA-APO3G (Fig. 3A). The effect on levels of integrated viral DNA by Δ*vif* virus produced in the presence of 4 μg of pcDNA-APO3G could not be determined because the Alu-LTR PCR DNA products were below the detection limit of the assay (data not shown).

Ligation of viral DNA ends that fail to integrate results in the formation of 2-LTR circles, and an increase in 2-LTR circles is used as a marker for inhibition of integration (3, 43). To investigate whether the decrease in the levels of integrated viral DNA in the presence of A3G was associated with an increase in 2-LTR circles, we quantified the amounts of 2-LTR circles in infected cells at 24 h after infection. The amount of 2-LTR circles formed was expressed as a proportion of late RT products at 6 h; the amount of 2-LTR circles of Δ*vif* virus DNA in the absence of A3G was set at 100% (Fig. 3B). In the presence of A3G, formation of 2-LTR circles of the Δ*vif* virus DNA was about twofold lower than in the absence of A3G ($P = 0.12$; *t* test). This observation suggested that the decrease in the levels of integrated viral DNA in the presence of A3G was not associated with an increase in the formation of 2-LTR circles.

We hypothesized that A3G induces a decrease in the efficiency of 2-LTR circle formation as well as provirus formation, which would explain the absence of an increase in 2-LTR circles that is sometimes associated with inhibition of integration. To determine if A3G affects 2-LTR circle formation, we infected 293T cells with an HIV-1 strain that had an inactivating mutation (D64E) in the catalytic site of integrase (IN) which results in significant inhibition of viral DNA integration (43). Since the D64E mutant virus expresses the Vif protein,

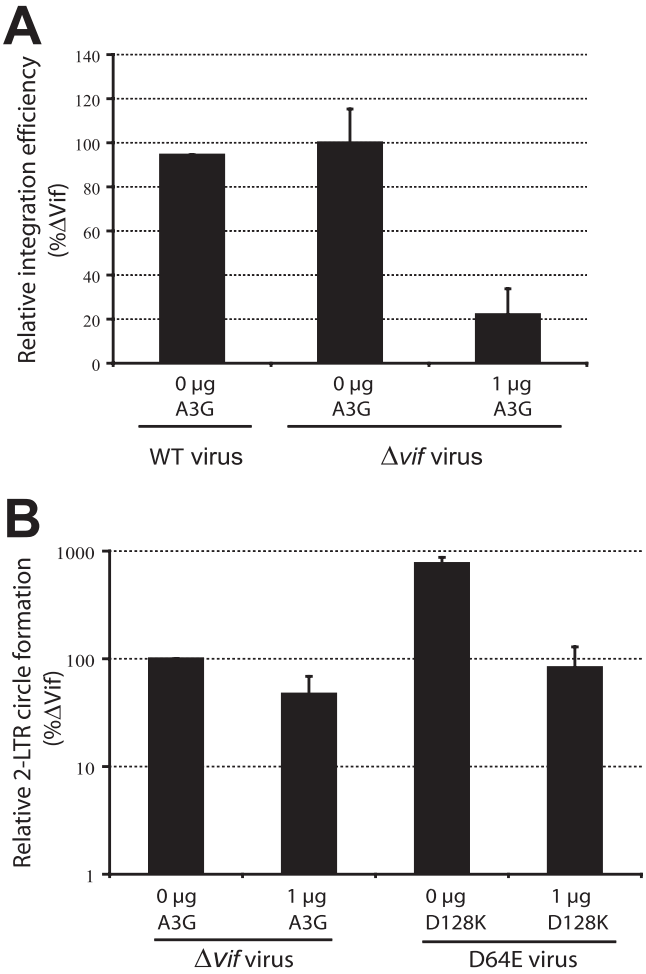

FIG. 3. Effect of A3G on integration efficiency and 2-LTR circle formation. (A) Relative integration efficiency of wild-type (WT) or Δ*vif* virus in the absence or presence of 1 μg of pcDNA-APO3G. The integration efficiency was determined as the proportion of late RT product at 6 h after infection that forms integrated proviruses 5 days after infection (AluPCR-5d/U5Ψ-6 h). The integration efficiency of Δ*vif* virus in the absence of A3G was set to 100%; the U5Ψ (6 h) copy numbers were 208,600 and 307,093, and the AluPCR (5 days) copy numbers were 35,862 and 27,349 for two independent experiments after adjustment for input DNA as determined by quantifying host PBGD gene copy numbers. The copy numbers for Δ*vif* virus in the presence of A3G for U5Ψ (6 h) were 43,300 and 28,201 and for AluPCR (5 days) were 655 and 995, respectively. (B) Relative 2-LTR circle formation in cells infected with Δ*vif* or D64E virus in the absence or presence of 1 μg of pcDNA-APO3G or pcDNA-D128K. Formation of 2-LTR circles was determined as the proportion of late RT product at 6 h after infection (2-LTR circles/U5Ψ-6 h). Formation of 2-LTR circles by Δ*vif* virus in the absence of A3G was set to 100%. Error bars in both graphs represent the standard errors of the means of two independent experiments.

we used an A3G mutant (D128K) that is Vif resistant (51). As expected, 2-LTR circle formation in cells infected with the D64E mutant virus was approximately 10-fold higher than control Δ*vif* virus in the absence of A3G. In the presence of A3G, the D64E mutant virus DNA formed 2-LTR circles with approximately 10-fold lower efficiency than in the absence of A3G. The result indicated that A3G decreased the efficiency of 2-LTR circle formation as well as provirus formation and could partly explain the absence of an increase in 2-LTR circle formation despite the reduction in provirus formation.

The decrease in provirus formation in the presence of A3G is dependent on a functional C-terminal zinc-binding domain. Several studies have shown that the catalytic activity of A3G is essential for its antiviral activity (26, 40). However, recent studies have shown that mutation of the conserved residues in CD2 does not significantly affect the ability of A3G or APOBEC3F to block virus replication, suggesting the existence of an antiretroviral mechanism independent of cytidine deamination activity (2, 31). To determine if the decrease in the levels of viral DNA in the presence of A3G is dependent on a functional cytidine deamination domain, we investigated the effect of two CD2 mutants, C288S and E259Q, on viral DNA replication, 2-LTR circle formation, and integration efficiency. Transfection with 1 or 4 μg of the mutant A3G-expressing plasmids had minimal or no effect on the infectivity of Δ*vif* virus (Fig. 4A) compared with a 35-fold or 1,000-fold decrease observed using wild-type pcDNA-APO3G, respectively (Fig. 1A). Transfection with 12 μg of mutant A3G-expressing plasmids resulted in a modest sevenfold reduction in virus replication with the C288S mutant, whereas the E259Q mutant had a minimal effect on virus replication. Consistent with the absence of an effect on viral infectivity, viral DNA levels in cells infected with Δ*vif* virus produced in the presence of 1 and 4 μg of both mutant A3G-expressing plasmids and 12 μg of the E259Q mutant A3G-expressing plasmid showed little or no effect (Fig. 4B) (one- to threefold). In the presence of 12 μg of the C288S mutant A3G-expressing plasmid, viral DNA levels were reduced sixfold. In contrast to wild-type pcDNA-APO3G (Fig. 3A), cotransfection with 1, 4, and 12 μg of the mutant-expressing plasmids did not significantly reduce integration efficiency (Fig. 4C). We also did not observe a statistically significant difference in the formation of 2-LTR circles for viruses produced in the presence of mutant A3G-expressing plasmids (Fig. 4D). Finally, the expression and Δ*vif* virion incorporation of CD2 mutants were determined by Western blotting analysis (Fig. 4E). Cotransfection of cells with 12 μg of the mutant A3G-expressing plasmids resulted in significantly higher levels of A3G virion incorporation, indicating that the diminished capacity of the CD2 mutants to inhibit viral DNA synthesis and integration efficiency was not due to a defect in expression or virion incorporation.

A3G inhibits PIC integration activity in vitro. To probe the mechanism by which A3G reduced the levels of integrated HIV-1 viral DNA, we isolated PICs from the cytoplasm of infected cells at 7 h after infection and determined their ability to integrate into an exogenous template DNA in vitro using a previously described real-time PCR assay (25). As described for the determination of in vivo integration efficiencies, the in vitro PIC activities were normalized to the levels of U5Ψ late RT products present in each sample as determined by real-time PCR quantification.

The integration efficiencies of PICs isolated from cells infected with wild-type virus in the presence or absence of A3G and that of PICs isolated from cells infected with Δ*vif* virus in the absence of A3G were similar (Fig. 5). However, the activity of PICs isolated from cells infected with Δ*vif* virus in the presence of A3G was decreased ninefold compared to Δ*vif* virus in the absence of A3G. In contrast, PICs isolated from cells infected with Δ*vif* virus produced in the presence of the C288S and E259Q A3G mutants displayed integration activities similar to those of PICs isolated from cells infected with wild-type virus. The data indicate that A3G's effect on the capacity of viral DNA to carry out integration occurs in the cytoplasm before the viral DNA encounters host cell DNA and that it is dependent on either cytidine deamination activity or an intact C-terminal domain structure.

A3G affects the specificity and efficiency of primer tRNA processing. HIV-1 DNA integration is a two-step reaction involving a 3′ processing reaction and a DNA strand transfer reaction (36). The 3′ processing reaction, which occurs soon after DNA synthesis and can be detected in the cytoplasm, entails the removal of GT dinucleotides from the 3′ ends. Mutations at the catalytic site of HIV-1 IN that abolish 3′ processing result in an increase in the proportion of unprocessed viral DNA ends and a block to viral DNA integration (43). To determine if A3G affects 3′ processing, we examined the U5 viral DNA end from cells infected with Δ*vif* virus in the presence or absence of A3G by Southern blotting analysis using a plus-strand DNA-specific riboprobe (Fig. 6A). Cytoplasmic DNA was isolated from infected cells at 6 h after infection, and U5Ψ late RT products were quantified. The cytoplasmic DNAs were normalized for the late RT products (3×10^7 copies) and digested with HindIII.

As expected, digestion of the HIV-1 unintegrated viral DNA with HindIII generated two fragments from the U5 end plus-strand DNA that completed synthesis: a 105-nucleotide (nt) fragment that did not undergo 3′ processing and a 103-nt fragment that underwent 3′ processing (Fig. 6B). Quantification of the intensities of the 103-nt and 105-nt bands was performed in two independent experiments; the intensities of the 103-nt band, which were similar in the presence and absence of A3G, were approximately 44% and 57%, respectively, of those of the total completed viral DNA ends (103-nt band plus 105-nt band). This observation suggested that A3G did not directly inhibit the 3′ processing reaction catalyzed by IN.

In addition to the 103-nt and 105-nt bands, a 122-nt fragment was also generated from plus-strand strong-stop DNA (+SSS DNA) that includes the primer binding site (PBS) sequence; this product results from copying of the primer tRNA at the 3′ end of the LTR (43). Intriguingly, this fragment was approximately sixfold more intense in the presence of A3G. The increase in intensity of this band suggested that A3G reduced the efficiency of primer tRNA cleavage and removal, which resulted in a reduced efficiency of +SSS DNA transfer. In addition, it is possible that the inhibition of primer tRNA processing resulted in the copying of the primer tRNA after +SSS DNA transfer, resulting in the formation of a 17-nt extension at the U5 end of the plus-strand viral DNA. Interestingly, an additional 111-nt band was observed in the presence of A3G but not in the absence of A3G. We hypothesize that this fragment was generated by copying of a partially

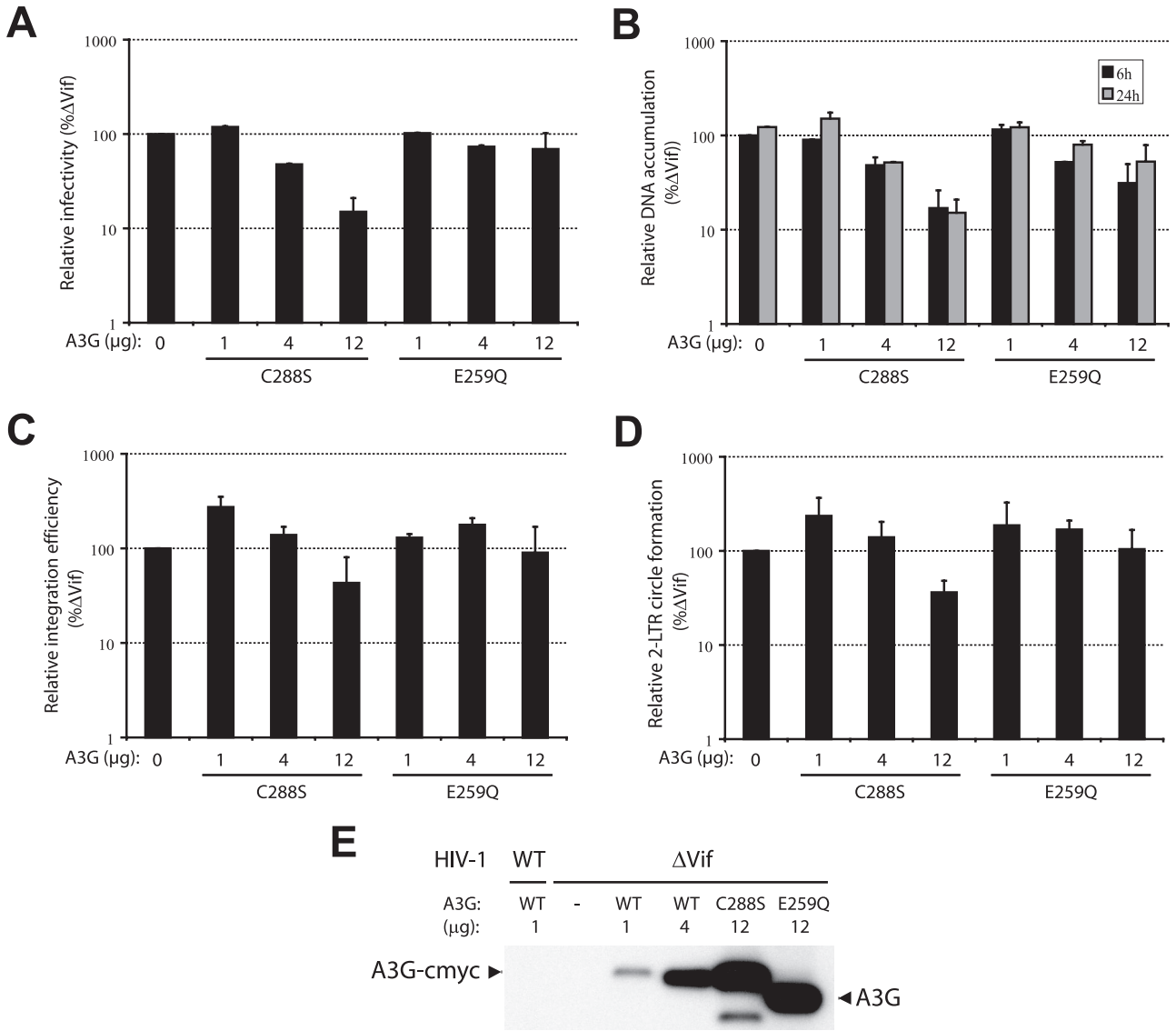

FIG. 4. Effect of CD2 mutants on infectivity, viral DNA replication, and integration. (A) Flow cytometry analysis of the effects of different amounts of A3G CD2 mutants, C288S and E259Q, on replication of Δ*vif* virus. The viruses were produced in the absence or presence of 1, 4, or 12 μg of C288S and E259Q mutant A3G-expressing plasmids by transfection of 293T cells. The MOI was determined from the proportion of GFP^+ cells after infection of 293T cells; the proportion of GFP^+ cells after infection with Δ*vif* virus in the absence of A3G ranged from 48.5 to 86.3% (MOI set to 100%). (B) Relative amounts of late RT products determined at 6 h (black bars) or 24 h (gray bars) postinfection with Δ*vif* virus in the absence or presence of 1, 4, or 12 μg of C288S or E259Q mutant A3G-expressing plasmids. The copy numbers of viral DNA that accumulated in cells infected with Δ*vif* virus in the absence of A3G were set to 100%; these copy numbers ranged from 8,839 to 14,367. (C) Relative integration efficiencies of Δ*vif* virus in the absence or presence of 1, 4, or 12 μg of C288S or E259Q mutant A3G-expressing plasmids. The integration efficiency was determined as the proportion of late RT product at 6 h after infection that form integrated proviruses 5 days after infection (AluPCR-5d/U5Ψ-6 h); the integration efficiency of Δ*vif* virus in the absence of A3G was set to 100%. (D) Relative 2-LTR-circle formation in cells infected with Δ*vif* virus in the absence or presence of 1, 4, or 12 μg of C288S and E259Q mutant A3G-expressing plasmids. Formation of 2-LTR circles was determined as the proportion of late RT product at 6 h after infection (2-LTR circles/U5Ψ-6 h); formation of 2-LTR circle by Δ*vif* virus in the absence of A3G was set to 100%. Error bars in all graphs represent the standard errors of the means of two independent experiments. (E) Western blotting analysis of viral lysates obtained from cells cotransfected with wild-type (WT) or Δ*vif* HIV-1 vectors along with wild-type A3G or A3G mutants C288S and E259Q. The wild-type and C288S mutant A3G proteins have a C-terminal c-*myc* tag and are labeled A3G-cmyc; the E259Q mutant A3G protein does not have a tag and is labeled A3G. The unlabeled band in the C288S lane is most likely a degradation product.

cleaved primer tRNA after +SSS DNA transfer, resulting in the formation of a 6-nt extension at the U5 end of the plus-strand viral DNA. Taken together, these results suggested that the presence of A3G interferes with cleavage and removal of the primer tRNA from the 3′ end of viral DNA, resulting in the formation of aberrant viral DNA ends that are not suitable substrates for the integration reaction.

Effect of A3G on the nature of 2-LTR circle junctions. To gain further insight into the mechanism by which A3G decreases provirus formation, we examined the nature of 2-LTR

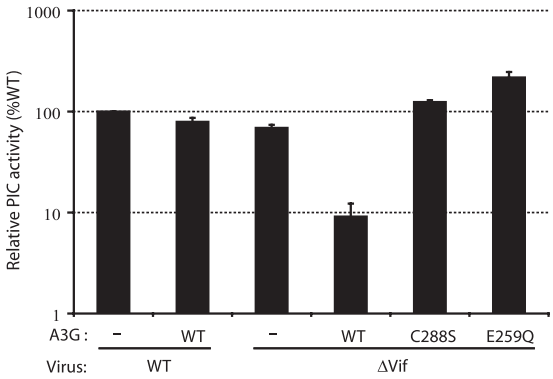

FIG. 5. Effect of A3G on PIC integration activity. Relative integration activity levels of PICs isolated from cells infected with wild-type (WT) or Δ*vif* virus in the absence or presence of 1 μg of WT pcDNA-APO3G or 12 μg of C288S or E259Q mutant A3G-expressing plasmids. All PIC integration activity levels were normalized to the amounts of viral DNA in the samples, as determined by quantitative real-time PCR of late RT products. The PIC integration activity level of WT virus in the absence of A3G was set to 100%. Error bars indicate the standard errors of the means of duplicate real-time quantitative PCR assays.

circle junctions. Unintegrated DNAs were isolated from cells infected with wild-type or Δ*vif* virus in the presence of A3G 24 h after infection, and 2-LTR circle junctions were PCR amplified, cloned, and sequenced. The loss of viral DNA at the ends of the LTRs because of failure to complete plus-strand DNA synthesis or through degradation would be expected to result in decreased integration efficiency and an increase in 2-LTR circles with deletions at their junctions. The proportions of wild-type junctions, deletions, insertions, and mutations were not statistically different among 105 wild-type and 90 Δ*vif* virus-derived 2-LTR circle junction sequences (Table 1). In addition, no differences in the sizes of the deletions or the locations of the deletion junctions were apparent (see Fig. S1 and S2 in the supplemental material). As expected, and consistent with previous reports (13, 14, 23, 26, 52, 54), the 2-LTR circle junction sequences obtained from cells infected with the Δ*vif* virus produced from A3G-expressing cells had G-to-A hypermutations in the 3′ LTR and C-to-T hypermutations in the 5′ LTR.

To probe the effects of A3G on the cleavage and removal of the primer tRNA, we examined the sequences inserted at the circle junctions in the presence of A3G (Fig. 6C). Interestingly, we noted that 3 of 10 insertions at the 2-LTR circle junctions constituted a 6-nt sequence derived from the 5′ end of the PBS. This insert sequence is consistent with the aberrant 111-nt band observed in the Southern analysis of the U5 DNA ends in the presence of A3G (Fig. 6B). This 6-nt insert was not present in any of the 22 clones of 2-LTR circle junction sequences containing inserts at the viral DNA ends from cells infected with Δ*vif* virus in the absence of A3G (see Fig. S1 in the supplemental material). Taken together, these data suggest that A3G causes aberrant cleavage of the primer tRNA from the 3′ end of viral DNA that generates atypical viral DNA ends that are incapable of completing integration.

A3G inhibits plus-strand DNA transfer. The increase in +SSS DNA in the presence of A3G suggested that A3G-induced reduction in primer tRNA processing could result in inhibition of plus-strand DNA transfer. To determine if A3G causes a defect in plus-strand DNA transfer, we compared the amount of U5Ψ DNA products (synthesized after plus-strand DNA transfer) to that of U3U5 DNA products (synthesized after minus-strand DNA transfer but before plus-strand DNA transfer) in the presence and absence of A3G using real-time PCR (Fig. 7A). The results showed a twofold decrease in plus-strand DNA transfer in Δ*vif* virus produced in the presence of 1 μg of pcDNA-APO3G and a fourfold decrease in the presence of 4 μg of pcDNA-APO3G (Fig. 7B). It is important to note that the HDV-EGFP DNA standard used for real-time PCR quantitation contained two LTRs containing the U3U5 DNA and one copy of the U5Ψ DNA. Viral DNAs that have completed plus-strand DNA transfer and DNA synthesis are expected to contain two U3U5 sequences and one U5Ψ sequence per genome; however, viral DNAs that did not undergo plus-strand DNA transfer are expected to contain only one U3U5 sequence and no U5Ψ sequences. As a result, when plus-strand DNA transfer is inhibited, the U3U5 copy numbers are likely to be underestimated, resulting in an underestimation of the plus-strand DNA transfer defect by as much as twofold. The presence of A3G did not affect minus-strand DNA transfer, as determined by comparison of U3U5 RT products to RU5 RT products (synthesized before minus-strand DNA transfer) (Fig. 7). These results suggest that A3G inhibits plus-strand DNA transfer by affecting the efficiency of primer tRNA processing. Although the twofold decrease in plus-strand DNA transfer could be an underestimate, the reduction in plus-strand DNA transfer does not fully account for an overall sevenfold reduction in DNA synthesis.

DISCUSSION

The results of these studies show for the first time that A3G can suppress HIV-1 replication by producing viral DNAs that are defective for plus-strand DNA transfer and integration. The conclusion that viral DNAs are defective for plus-strand DNA transfer is supported by Southern analysis of unintegrated viral DNAs as well as quantitative real-time PCR analysis. The conclusion that viral DNAs are defective for integration is supported by observations that integration of viral DNA into the chromatin of infected cells is reduced in the presence of A3G and that PICs produced in the presence of A3G exhibit a defect in their in vitro integration activity. This defect in integration activity was correlated with aberrant DNA structures at the ends of the 3′ LTR. The observation that the proportions of normal 3′ LTR DNA ends were similar in the presence and absence of A3G suggests that other defects in the PICs also exist and contribute to inhibition of integration. The fivefold decrease in provirus formation during experiments in which infectivity was reduced 35-fold suggests that this is a quantitatively important mechanism of viral inhibition.

Analysis of unintegrated viral DNA by Southern blotting supports a novel mechanism by which A3G inhibits the efficiency of viral DNA integration. The Southern analysis showed that in the presence of A3G, a large proportion of the U5 DNA ends possessed a 6-nt extension (111-nt band in Fig. 6B); in addition, the presence of A3G increased the proportion of +SSS DNA (122-nt band in Fig. 6B). These observations are

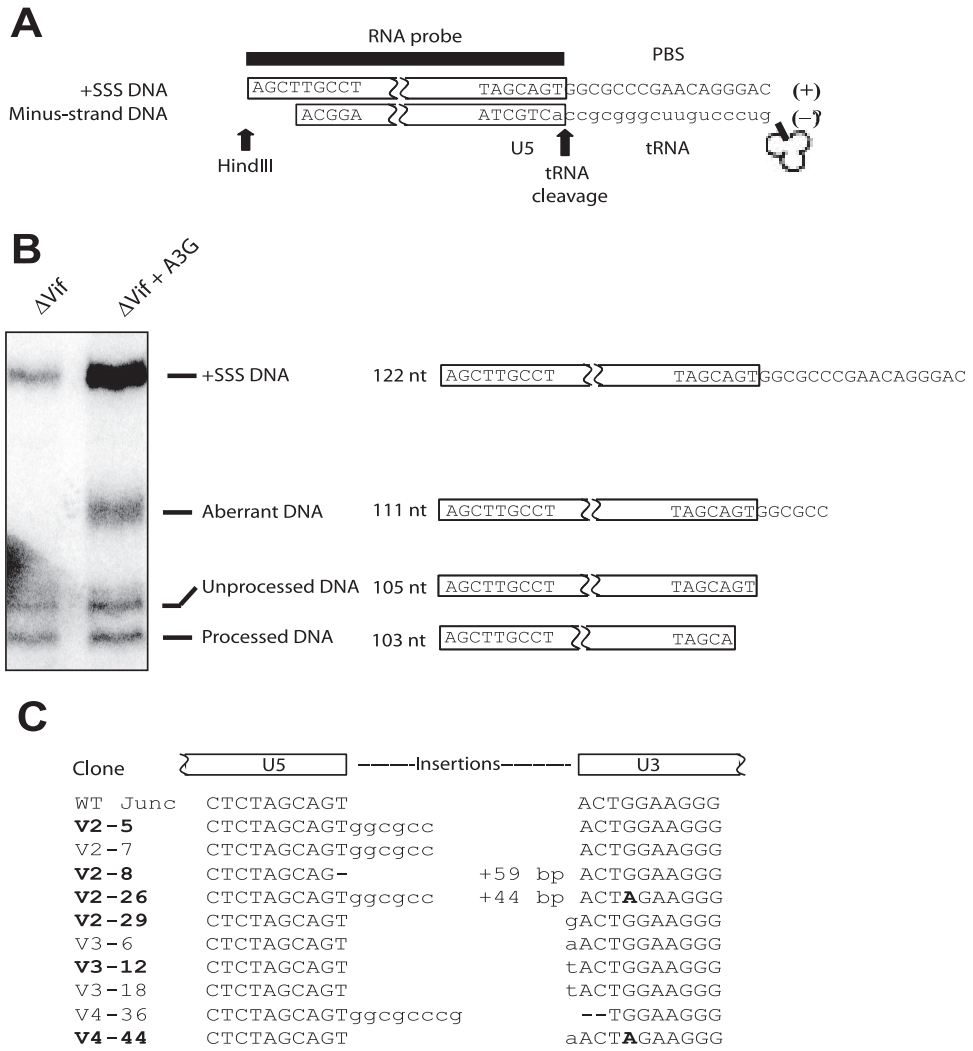

FIG. 6. Southern blotting analysis of U5 viral DNA ends of the 3′ LTR in the absence or presence of A3G. (A) Reverse transcription products were detected after HindIII digestion by an RNA probe that hybridizes to the plus strand of U5 end HIV-1 DNA (thick line). The primer tRNA sequence is shown in lowercase letters while the rest of the tRNA is shown as a clover leaf. DNA sequences at the HindIII digestion site and at the U5 end as well as the PBS sequence are shown in uppercase letters. (B) Southern analysis of plus-strand DNA products generated after HindIII digestion of cytoplasmic DNA harvested 6 h after Δ*vif* HIV-1 infection in the presence or absence of A3G. The amounts of viral DNA products were quantified by real-time PCR of late RT products, and 3×10^7 copies of late RT products from each sample were analyzed. The lanes are labeled according to the virus used for infection. Unprocessed plus-strand DNA generated a 105-nt fragment (labeled unprocessed DNA), while the plus-strand DNA ends that underwent 3′ processing generated a 103-nt fragment (labeled processed DNA). The fragment of plus-strand strong-stop DNA (labeled +SSS DNA) is 122 nt in length, and the plus-strand DNA fragment resulting from copying of an aberrantly processed primer tRNA is approximately 111 nt in length (labeled aberrant DNA). The sizes of the processed and unprocessed bands were determined by the migration of specific 103- and 105-nt-long oligonucleotide markers as described previously (43), while the size of the other bands was determined by the migration of end-labeled commercial DNA molecular weight markers. (C) Analysis of 2-LTR circle junction clones with inserted sequences obtained from cells infected with Δ*vif* HIV-1 in the presence of A3G. Schematic of U5 and U3 ends and inserted sequence is shown at the top with the wild-type (WT) junction DNA sequence (WT Junc). The circle junction sequences of the clones are aligned to the wild-type sequence, and the inserted sequences are shown in lowercase letters. The names of clones that contained G-to-A hypermutations within the sequenced 336-bp fragment are shown in boldface. The dashes represent deleted nucleotides, and the boldfaced nucleotides are G-to-A hypermutations.

consistent with the interpretation that A3G interferes with the processing and removal of the primer tRNA from the U5 minus-strand DNA end. During normal reverse transcription, the primer tRNA is cleaved intact 5′ of the adenosine 5′ phosphate at the RNA-DNA junction (Fig. 6A; see also references 33 and 42). We hypothesize that the aberrant primer tRNA cleavage still allows plus-strand DNA transfer to occur by hybridization of the remaining 11-nt single-stranded region of the PBS to the minus-strand DNA; completion of plus-strand DNA synthesis results in the formation of viral DNA that contains an additional 6 nt at the U5 end. Sequencing of the 2-LTR circle junctions that were formed in the presence of A3G revealed three circle junctions with this 6-nt insertion, confirming their presence at the end of some of the completed viral DNAs. We hypothesize that the 6-nt extension interferes with the 3′ processing reaction catalyzed by HIV-1 IN, result-

TABLE 1. Analysis of 2-LTR circle junctions

Nature of circle junction	Wild type + A3G		Δ*vif* + A3G	
	No. of circle junctions	Frequency (mean % ± SEM)[a]	No. of circle junctions	Frequency (mean % ± SEM)[a]
Wild type	27	27 ± 7[b]	34	38 ± 4[b]
Deletion	56	53 ± 4[c]	44	49 ± 2[c]
Insertion	22	21 ± 6[d]	10	11 ± 3[d]
Substitution[e]	0	0	2	2 ± 3
Total	105	100	90	100

[a] Mean for three independent experiments ± standard errors of the means (SEM).
[b] $P = 0.14$; *t* test.
[c] $P = 0.30$; *t* test.
[d] $P = 0.07$; *t* test.
[e] Only substitutions at the GT/AC dinucleotides at the circle junctions are shown.

ing in inhibition of integration. However, A3G did not directly inhibit the 3′ processing reaction because the proportion of completed viral DNA ends (the 105-nt and 103-nt fragments in Fig. 6B) that underwent 3′ processing was not significantly different in the presence or absence of A3G. Furthermore, we did not observe an increase in the frequency of wild-type 2-LTR circle junctions in the presence of A3G that is associated with inhibition of the 3′ processing reaction (43).

It is possible that the +SSS DNA can carry out plus-strand DNA transfer in the absence of primer tRNA removal, albeit at a lower efficiency. This could result in the formation of a completed viral DNA containing a 17-nt extension at the U5 DNA end. The 17-nt extension could also interfere with the 3′ processing reaction and integration catalyzed by HIV-1 IN.

Our Southern analysis data indicate that A3G does not decrease provirus formation by inducing degradation of the 3′ LTR DNA end. The amounts of completed viral DNA ends detected by Southern analysis in the presence or absence of A3G were very similar, indicating that the presence of A3G did not result in DNA end degradation. In addition, the Southern analysis did not reveal any fragments smaller than 103 nt in the presence of A3G that could indicate degradation of the 3′ LTR DNA end. This observation is also consistent with our analysis of DNA accumulation in the presence or absence of UNG2 in the virus producer cells or target cells of infection. Our results indicated that inhibition of UNG2 activity did not significantly affect the accumulation of viral DNA and confirm recent observations that UNG2 does not influence HIV-1 replication in dividing cells (7, 19). In previous studies, the defect in Δ*vif* virus replication has been attributed to degradation of viral DNA (26, 41, 46). The results of these studies were consistent with our results; it was noted that the amount of integrated viral DNA was significantly less than the amount of reverse-transcribed viral DNA. However, in the previous studies, this difference was attributed to degradation of the viral DNA before integration, while our studies show that the reduction in integration efficiency is not the result of viral DNA degradation but is associated with aberrant viral DNA ends. We did not observe an increase in the formation of 2-LTR circles that is sometimes associated with inhibition of viral DNA integration (43). However, our analysis of the IN-defective HIV-1 D64E mutant clearly shows that in the presence of A3G 2-LTR circle formation is decreased. Thus, the effect of A3G on both viral DNA integration and 2-LTR circle formation explains the absence of an increase in 2-LTR circle formation.

The observation that catalytic site mutants of A3G had little or no effect on levels of integrated viral DNA strongly suggests that the cytidine deamination activity or a functional CD2 of A3G is required for the reduction in provirus formation. G-to-A hypermutations near the viral DNA ends could contribute to the reduced efficiency of provirus formation. Because A3G reduced both the levels of integrated viral DNA and 2-LTR circles, the extent of G-to-A hypermutations that occur near the ends of viral DNA that did not integrate cannot be determined from the sequencing analysis of 2-LTR circle junctions. It is also possible that A3G physically blocks the cleavage of the primer tRNA by binding to the viral DNA ends. Based on recent findings that A3G exhibits processivity in the 3′ to 5′ direction on target DNA (5), A3G could migrate toward the 5′ direction of the minus-strand DNA and, once it reaches the 5′ end, remain bound to the template, thereby interfering with primer tRNA processing and removal. Thus, the CD2 mutants may interfere with the

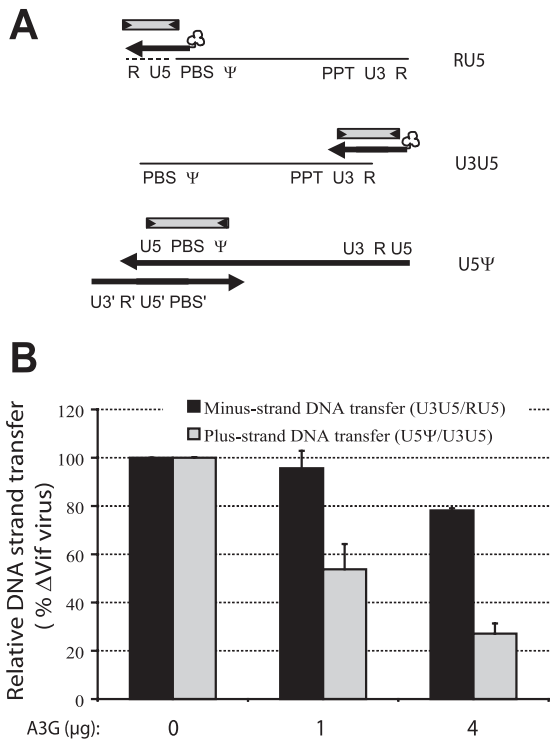

FIG. 7. Effect of A3G on minus- or plus-strand DNA transfer of Δ*vif* HIV-1. (A) Schematic showing the locations of RU5, U3U5, and U5ψ primer-probe sets (shaded gray boxes containing arrows) used to determine the efficiency of minus- or plus-strand DNA transfer. The thin line represents viral RNA, the thick line represents viral DNA, and the clover leaf represents the primer tRNA. (B) The bar graph shows relative minus- or plus-strand DNA transfer efficiencies in the absence or presence of either 1 or 4 μg of transfected pcDNA-APO3G at 6 h after infection. Minus-strand DNA transfer efficiency was determined by calculating the proportion of RU5 RT products that formed U3U5 RT products, whereas plus-strand DNA transfer was determined by calculating the proportion of U3U5 RT products that subsequently formed U5ψ RT products. The efficiency of minus- or plus-strand DNA transfer in the presence of A3G was then compared to that in the absence of A3G (set at 100%). Error bars represent standard errors of the means of two independent experiments.

processive movement and/or DNA binding of A3G, thereby preventing inhibition of integration. Finally, it is possible that A3G binds to or modifies the primer tRNA to inhibit its cleavage and removal by RNase H.

Recent studies have shown that inhibition of Δ*vif* virus replication by A3G is primarily due to a block in viral DNA synthesis (2, 15). In contrast, our results indicated that a five- to sevenfold decrease in viral DNA synthesis occurs during experiments in which overall viral replication was inhibited 35-fold. These different results could be due to the difference in the amounts of A3G expressed in these two studies; in the previous studies, an A3G/HIV-1 vector molar ratio of 1:1 was used, while in our studies, transfection with 1 μg of pcDNA-APO3G results in a molar ratio of 1:5. We recently showed that virions produced from activated primary $CD4^+$ T cells contain exceedingly small amounts of A3G (7 ± 4 molecules) compared to those present in virions produced from some transiently transfected 293T cells (50). We have also shown that transfection of 293T cells with 1 μg of pcDNA-APO3G (molar ratio, 1:5) results in virions that package about twofold more cytidine deamination activity than virions produced in activated primary $CD4^+$ T cells (50). Since the expression of A3G in primary cells can be upregulated three- to fourfold by interferons (6, 35), we surmise that the reduction in provirus formation and viral DNA synthesis that we observed from transfection with 1 μg of pcDNA-APO3G results from A3G expression levels that are within twofold of those found in primary $CD4^+$ T cells. The observed twofold reduction in plus-strand DNA transfer partially accounts for the five- to sevenfold inhibition of DNA synthesis. The remainder of the inhibition by A3G of viral DNA synthesis could be due to an effect on the initiation of minus-strand DNA synthesis (11).

Our studies indicate that the observed five- to sevenfold reduction in DNA synthesis together with the fivefold reduction in integration efficiency are sufficient to explain most of the 35-fold reduction in HIV-1 infectivity. Nevertheless, G-to-A hypermutation most likely inactivates viral genes and suppresses expression of functional viral proteins from proviruses, further inhibiting HIV-1 replication.

In summary, these studies advance our understanding of the mechanisms that A3G uses to mediate retrovirus restriction and reveal for the first time that A3G reduces the efficiency and specificity of primer tRNA processing and removal, thereby producing viral DNA ends that are defective for plus-strand DNA transfer and integration. Further elucidation of the mechanism by which A3G interferes with HIV-1 integration could provide new opportunities for the design of specific inhibitors of HIV-1 integration.

ACKNOWLEDGMENTS

We especially thank Wei-Shau Hu for intellectual input throughout the project and Guylaine Hache and Amy Briggs for key DNA constructs. We also thank David Derse, Wei-Shau Hu, and April Schumacher for valuable discussions and critical comments during manuscript preparation and Anne Arthur for expert editorial assistance during manuscript preparation.

This research was supported in part by the Intramural Research Program of the NIH, National Cancer Institute, Center for Cancer Research. This project was also funded in part by National Institutes of Health grants AI39394 (A.E.), AI064046 (R.S.H.), GM56615 (L.M.M.), and AI57735 (L.M.M.) and by funds from the National Cancer Institute, National Institutes of Health, under contract N01-CO-12400 (R.G.).

The content of this publication does not necessarily reflect the views or policies of the Department of Health and Human Services, nor does mention of trade names, commercial products, or organizations imply endorsement by the U.S. Government.

REFERENCES

1. **Beale, R. C., S. K. Petersen-Mahrt, I. N. Watt, R. S. Harris, C. Rada, and M. S. Neuberger.** 2004. Comparison of the differential context-dependence of DNA deamination by APOBEC enzymes: correlation with mutation spectra in vivo. J. Mol. Biol. **337:**585–596.
2. **Bishop, K. N., R. K. Holmes, and M. H. Malim.** 2006. Antiviral potency of APOBEC proteins does not correlate with cytidine deamination. J. Virol. **80:**8450–8458.
3. **Buckman, J. S., W. J. Bosche, and R. J. Gorelick.** 2003. Human immunodeficiency virus type 1 nucleocapsid Zn^{2+} fingers are required for efficient reverse transcription, initial integration processes, and protection of newly synthesized viral DNA. J. Virol. **77:**1469–1480.
4. **Butler, S. L., M. S. Hansen, and F. D. Bushman.** 2001. A quantitative assay for HIV DNA integration in vivo. Nat. Med. **7:**631–634.
5. **Chelico, L., P. Pham, P. Calabrese, and M. F. Goodman.** 2006. APOBEC3G DNA deaminase acts processively 3′→5′ on single-stranded DNA. Nat. Struct. Mol. Biol. **13:**392–399.
6. **Chen, K., J. Huang, C. Zhang, S. Huang, G. Nunnari, F. X. Wang, X. Tong, L. Gao, K. Nikisher, and H. Zhang.** 2006. Alpha interferon potently enhances the anti-human immunodeficiency virus type 1 activity of APOBEC3G in resting primary CD4 T cells. J. Virol. **80:**7645–7657.
7. **Chen, R., E. Le Rouzic, J. A. Kearney, L. M. Mansky, and S. Benichou.** 2004. Vpr-mediated incorporation of UNG2 into HIV-1 particles is required to modulate the virus mutation rate and for replication in macrophages. J. Biol. Chem. **279**:28419–28425.
8. **Conticello, S. G., R. S. Harris, and M. S. Neuberger.** 2003. The Vif protein of HIV triggers degradation of the human antiretroviral DNA deaminase APOBEC3G. Curr. Biol. **13:**2009–2013.
9. **Di Noia, J., and M. S. Neuberger.** 2002. Altering the pathway of immunoglobulin hypermutation by inhibiting uracil-DNA glycosylase. Nature **419:**43–48
10. **Fitzgibbon, J. E., S. Mazar, and D. T. Dubin.** 1993. A new type of G→A hypermutation affecting human immunodeficiency virus. AIDS Res. Hum. Retrovir. **9:**833–838.
11. **Guo, F., S. Cen, M. Niu, J. Saadatmand, and L. Kleiman.** 2006. Inhibition of formula-primed reverse transcription by human APOBEC3G during human immunodeficiency virus type 1 replication. J. Virol. **80:**11710–11722.
12. **Hache, G., M. T. Liddament, and R. S. Harris.** 2005. The retroviral hypermutation specificity of APOBEC3F and APOBEC3G is governed by the C-terminal DNA cytosine deaminase domain. J. Biol. Chem. **280:**10920–10924.
13. **Harris, R. S., K. N. Bishop, A. M. Sheehy, H. M. Craig, S. K. Petersen-Mahrt, I. N. Watt, M. S. Neuberger, and M. H. Malim.** 2003. DNA deamination mediates innate immunity to retroviral infection. Cell **113:**803–809.
14. **Harris, R. S., A. M. Sheehy, H. M. Craig, M. H. Malim, and M. S. Neuberger.** 2003. DNA deamination: not just a trigger for antibody diversification but also a mechanism for defense against retroviruses. Nat. Immunol. **4:**641–643.
15. **Holmes, R. K., F. A. Koning, K. N. Bishop, and M. H. Malim.** 2007. APOBEC3F can inhibit the accumulation of HIV-1 reverse transcription products in the absence of hypermutation: comparisons with APOBEC3G. J. Biol. Chem. **282:**2587–2595.
16. **Huthoff, H., and M. H. Malim.** 2005. Cytidine deamination and resistance to retroviral infection: towards a structural understanding of the APOBEC proteins. Virology **334:**147–153.
17. **Jarmuz, A., A. Chester, J. Bayliss, J. Gisbourne, I. Dunham, J. Scott, and N. Navaratnam.** 2002. An anthropoid-specific locus of orphan C to U RNA-editing enzymes on chromosome 22. Genomics **79:**285–296.
18. **Julias, J. G., A. L. Ferris, P. L. Boyer, and S. H. Hughes.** 2001. Replication of phenotypically mixed human immunodeficiency virus type 1 virions containing catalytically active and catalytically inactive reverse transcriptase. J. Virol. **75:**6537–6546.
19. **Kaiser, S. M., and M. Emerman.** 2006. Uracil DNA glycosylase is dispensable for human immunodeficiency virus type 1 replication and does not contribute to the antiviral effects of the cytidine deaminase APOBEC3G. J. Virol. **80:**875–882.
20. **Kao, S., H. Akari, M. A. Khan, M. Dettenhofer, X. F. Yu, and K. Strebel.** 2003. Human immunodeficiency virus type 1 Vif is efficiently packaged into virions during productive but not chronic infection. J. Virol. **77:**1131–1140.
21. **Klarmann, G. J., X. Chen, T. W. North, and B. D. Preston.** 2003. Incorporation of uracil into minus strand DNA affects the specificity of plus strand synthesis initiation during lentiviral reverse transcription. J. Biol. Chem. **278:**7902–7909.
22. **Kobayashi, M., A. Takaori-Kondo, Y. Miyauchi, K. Iwai, and T. Uchiyama.** 2005. Ubiquitination of APOBEC3G by an HIV-1 Vif-Cullin5-Elongin B-

Elongin C complex is essential for Vif function. J. Biol. Chem. **280:**18573–18578.
23. **Lecossier, D., F. Bouchonnet, F. Clavel, and A. J. Hance.** 2003. Hypermutation of HIV-1 DNA in the absence of the Vif protein. Science **300:**1112.
24. **Liddament, M. T., W. L. Brown, A. J. Schumacher, and R. S. Harris.** 2004. APOBEC3F properties and hypermutation preferences indicate activity against HIV-1 in vivo. Curr. Biol. **14:**1385–1391.
25. **Lu, R., N. Vandegraaff, P. Cherepanov, and A. Engelman.** 2005. Lys-34, dispensable for integrase catalysis, is required for preintegration complex function and human immunodeficiency virus type 1 replication. J. Virol. **79:**12584–12591.
26. **Mangeat, B., P. Turelli, G. Caron, M. Friedli, L. Perrin, and D. Trono.** 2003. Broad antiretroviral defence by human APOBEC3G through lethal editing of nascent reverse transcripts. Nature **424:**99–103.
27. **Mansky, L. M., S. Preveral, L. Selig, R. Benarous, and S. Benichou.** 2000. The interaction of vpr with uracil DNA glycosylase modulates the human immunodeficiency virus type 1 In vivo mutation rate. J. Virol. **74:**7039–7047.
28. **Mariani, R., D. Chen, B. Schrofelbauer, F. Navarro, R. Konig, B. Bollman, C. Munk, H. Nymark-McMahon, and N. R. Landau.** 2003. Species-specific exclusion of APOBEC3G from HIV-1 virions by Vif. Cell **114:**21–31.
29. **Mehle, A., B. Strack, P. Ancuta, C. Zhang, M. McPike, and D. Gabuzda.** 2004. Vif overcomes the innate antiviral activity of APOBEC3G by promoting its degradation in the ubiquitin-proteasome pathway. J. Biol. Chem. **279:**7792–7798.
30. **Navarro, F., B. Bollman, H. Chen, R. Konig, Q. Yu, K. Chiles, and N. R. Landau.** 2005. Complementary function of the two catalytic domains of APOBEC3G. Virology **333:**374–386.
31. **Newman, E. N., R. K. Holmes, H. M. Craig, K. C. Klein, J. R. Lingappa, M. H. Malim, and A. M. Sheehy.** 2005. Antiviral function of APOBEC3G can be dissociated from cytidine deaminase activity. Curr. Biol. **15:**166–170.
32. **Nikolenko, G. N., E. S. Svarovskaia, K. A. Delviks, and V. K. Pathak.** 2004. Antiretroviral drug resistance mutations in human immunodeficiency virus type 1 reverse transcriptase increase template-switching frequency. J. Virol. **78:**8761–8770.
33. **Omer, C. A., and A. J. Faras.** 1982. Mechanism of release of the avian retrovirus tRNATrp primer molecule from viral DNA by ribonuclease H during reverse transcription. Cell **30:**797–805.
34. **Pathak, V. K., and H. M. Temin.** 1990. Broad spectrum of in vivo forward mutations, hypermutations, and mutational hotspots in a retroviral shuttle vector after a single replication cycle: substitutions, frameshifts, and hypermutations. Proc. Natl. Acad. Sci. USA **87:**6019–6023.
35. **Peng, G., K. J. Lei, W. Jin, T. Greenwell-Wild, and S. M. Wahl.** 2006. Induction of APOBEC3 family proteins, a defensive maneuver underlying interferon-induced anti-HIV-1 activity. J. Exp. Med. **203:**41–46.
36. **Pommier, Y., and N. Neamati.** 1999. Inhibitors of human immunodeficiency virus integrase. Adv. Virus Res. **52:**427–458.
37. **Priet, S., N. Gros, J. M. Navarro, J. Boretto, B. Canard, G. Querat, and J. Sire.** 2005. HIV-1-associated uracil DNA glycosylase activity controls dUTP misincorporation in viral DNA and is essential to the HIV-1 life cycle. Mol. Cell **17:**479–490.
38. **Schrofelbauer, B., Q. Yu, S. G. Zeitlin, and N. R. Landau.** 2005. Human immunodeficiency virus type 1 Vpr induces the degradation of the UNG and SMUG uracil-DNA glycosylases. J. Virol. **79:**10978–10987.
39. **Sheehy, A. M., N. C. Gaddis, J. D. Choi, and M. H. Malim.** 2002. Isolation of a human gene that inhibits HIV-1 infection and is suppressed by the viral Vif protein. Nature **418:**646–650.
40. **Shindo, K., A. Takaori-Kondo, M. Kobayashi, A. Abudu, K. Fukunaga, and T. Uchiyama.** 2003. The enzymatic activity of CEM15/Apobec-3G is essential for the regulation of the infectivity of HIV-1 virion but not a sole determinant of its antiviral activity. J. Biol. Chem. **278:**44412–44416.
41. **Simon, J. H., and M. H. Malim.** 1996. The human immunodeficiency virus type 1 Vif protein modulates the postpenetration stability of viral nucleoprotein complexes. J. Virol. **70:**5297–5305.
42. **Smith, J. S., and M. J. Roth.** 1992. Specificity of human immunodeficiency virus-1 reverse transcriptase-associated ribonuclease H in removal of the minus-strand primer, tRNA(Lys3). J. Biol. Chem. **267:**15071–15079.
43. **Svarovskaia, E. S., R. Barr, X. Zhang, G. C. Pais, C. Marchand, Y. Pommier, T. R. Burke, Jr., and V. K. Pathak.** 2004. Azido-containing diketo acid derivatives inhibit human immunodeficiency virus type 1 integrase in vivo and influence the frequency of deletions at two-long-terminal-repeat-circle junctions. J. Virol. **78:**3210–3222.
44. **Thomas, J. A., T. D. Gagliardi, W. G. Alvord, M. Lubomirski, W. J. Bosche, and R. J. Gorelick.** 2006. Human immunodeficiency virus type 1 nucleocapsid zinc-finger mutations cause defects in reverse transcription and integration. Virology **353:**41–51.
45. **Vartanian, J. P., A. Meyerhans, B. Asjo, and S. Wain-Hobson.** 1991. Selection, recombination, and G→A hypermutation of human immunodeficiency virus type 1 genomes. J. Virol. **65:**1779–1788.
46. **von Schwedler, U., J. Song, C. Aiken, and D. Trono.** 1993. Vif is crucial for human immunodeficiency virus type 1 proviral DNA synthesis in infected cells. J. Virol. **67:**4945–4955.
47. **Voronin, Y. A., and V. K. Pathak.** 2004. Frequent dual initiation in human immunodeficiency virus-based vectors containing two primer-binding sites: a quantitative in vivo assay for function of initiation complexes. J. Virol. **78:**5402–5413.
48. **Wang, Z., and D. W. Mosbaugh.** 1989. Uracil-DNA glycosylase inhibitor gene of bacteriophage PBS2 encodes a binding protein specific for uracil-DNA glycosylase. J. Biol. Chem. **264:**1163–1171.
49. **Willetts, K. E., F. Rey, I. Agostini, J. M. Navarro, Y. Baudat, R. Vigne, and J. Sire.** 1999. DNA repair enzyme uracil DNA glycosylase is specifically incorporated into human immunodeficiency virus type 1 viral particles through a Vpr-independent mechanism. J. Virol. **73:**1682–1688.
50. **Xu, H., E. Chertova, J. Chen, D. E. Ott, J. D. Roser, W. S. Hu, and V. K. Pathak.** 2006. Stoichiometry of the antiviral protein APOBEC3G in HIV-1 virions. Virology **360:**247–256.
51. **Xu, H., E. S. Svarovskaia, R. Barr, Y. Zhang, M. A. Khan, K. Strebel, and V. K. Pathak.** 2004. A single amino acid substitution in human APOBEC3G antiretroviral enzyme confers resistance to HIV-1 virion infectivity factor-induced depletion. Proc. Natl. Acad. Sci. USA **101:**5652–5657.
52. **Yu, Q., R. Konig, S. Pillai, K. Chiles, M. Kearney, S. Palmer, D. Richman, J. M. Coffin, and N. R. Landau.** 2004. Single-strand specificity of APOBEC3G accounts for minus-strand deamination of the HIV genome. Nat. Struct. Mol. Biol. **11:**435–442.
53. **Yu, X., Y. Yu, B. Liu, K. Luo, W. Kong, P. Mao, and X. F. Yu.** 2003. Induction of APOBEC3G ubiquitination and degradation by an HIV-1 Vif-Cul5-SCF complex. Science **302:**1056–1060.
54. **Zhang, H., B. Yang, R. J. Pomerantz, C. Zhang, S. C. Arunachalam, and L. Gao.** 2003. The cytidine deaminase CEM15 induces hypermutation in newly synthesized HIV-1 DNA. Nature **424:**94–98.